AIAA JOURNAL
Vol. 38, No. 4, April 2000

Wake of a Self-Propelled Body, Part 1: Momentumless Wake

A. I. Sirviente*
University of Michigan, Ann Arbor, Michigan 48109-2145
and
V. C. Patel†
University of Iowa, Iowa City, Iowa 52242-1585

Experiments were performed in the turbulent boundary layer and near wake of an axisymmetric body propelled by a jet to study the evolution of the momentumless wake. Comparisons with measurements in the drag wake of the body (without the jet) and in the isolated jet provide an understanding of initial mixing between the two flows. Triple-sensor hot wires and multitube pressure probes were used to measure the mean velocity, turbulence, and pressure fields from the jet exit to a distance of over 15 jet diameters. It is found that the evolution of the wake takes place in three distinct stages: a zone close to the jet exit, about 4 jet diameters long, where the jet shear layer mixes with fluid from the wall region of the boundary layer; an intermediate region, about 12 jet diameters long, where there is mixing between the boundary layer and the jet up to the axis; and the third region where the two flows lose their identities to become a single shear layer and the mean flow acquires some of the characteristics of self-similar flows. However, the momentumless wake does not conform to the assumptions and results of classical similarity analysis.

I. Introduction

THE wake of a restrained axisymmetric body is characterized by a deficit of momentum flux. Momentumless wakes are generated by self-propelled bodies, the most common forms of propulsion being a jet or a propeller. Only a simple jet can provide streamwise momentum without swirl. This paper is concerned with this kind of momentumless wake. A previous paper[1] described the turbulent drag wake (with momentum deficit) of the same axisymmetric body used herein, whereas a companion paper[2] deals with the momentumless wake with swirl.

Measurements in axisymmetric, turbulent momentumless wakes were made by Ridjanovic,[3] Wang,[4] and Naudascher,[5] all of whom studied the flow behind a circular disk with a coaxial jet. Naudascher concluded that in the initial regime an axisymmetric momentumless wake is a free shear flow, but that far downstream it resembles decaying homogeneous turbulence. Schetz and Jakubowski[6] made measurements in the wake of an elongated jet-propelled body. The jet was rather large and annular in shape. More recently, the wake of a thin circular tube was experimentally investigated by Higuchi and Kubota[7] for different initial momentum conditions, including one with zero net momentum.

Similarity analysis of axisymmetric, turbulent momentumless wakes has been reported by a number of authors, but there is no consensus in the results. The predictions of similarity analysis depend on the turbulence model that is adopted, and consequently, on the approximations that are made in the model equations. Finson[8] used a second-order model and closed the system with an equation derived from the spectrum of turbulence kinetic energy k. Hassid[9] used a k–ε model, whereas Ferry and Piquet[10] employed the k equation and an eddy-viscosity model for the Reynolds stresses ($\overline{uv}$, $\overline{u^2}$, $\overline{v^2}$) and the rate of energy dissipation ε. Recently, Sirviente[11] used a Reynolds-stress transport model that includes a model ε equation, along with the experimental observation of negligible energy production in the transport equations. The results of the various analyses are summarized in Table 1, including those quoted by Tennekes and Lumley.[12] In Table 1, l and U are the length and velocity scales, respectively, and the subscript m denotes scales of the other quantities, namely, their maximum values.

This paper is concerned with experiments in the momentumless wake of an axisymmetric body. The chosen elongated shape closely resembles practical self-propelled bodies. It differs from shapes used in previous studies with respect to the initial conditions of the wake. Here, the wake is generated by mixing between a well-developed thick boundary layer on the body and a coaxial jet issuing from its tail. The present study documents the development of the momentumless wake from its origin in the mixing of these two distinct shear layers to its evolution into a single shear layer. Understanding of this mixing is facilitated by reference to measurements in the drag wake of the body[1] and the isolated jet issuing from the body tail.[11]

II. Design of Experiments

The axisymmetric body described by Sirviente and Patel[1] was also used for this study. The body has a length L of 143.45 cm, a maximum radius R of 6.95 cm, and a base diameter of 3.96 cm, allowing a coaxial jet of diameter $D = 3.90$ cm to be introduced from the tail. The boundary layer on the body was tripped by a 1.2-mm-diam wire located at a distance of 9.5 cm from the nose. Air for the jet was supplied through a 1.24-cm-diam pipe along the body axis entering the body at the nose.

The experiments were conducted in the 1.07-m octagonal, open test-section, return-circuit wind tunnel of the Iowa Institute of Hydraulic Research. Figure 1 shows the wind tunnel and model arrangement along with the cylindrical (x, r, θ) coordinate system used to report the data, where x is measured from the base. In the steady axisymmetric flow considered here, the mean and fluctuating velocity components in these coordinate directions are denoted by (U, V, W) and (u, v, w), respectively. The uniformity of mean velocity and turbulence intensity in the tunnel was investigated earlier.[13,14] The reported mean-flow uniformity in the test section was better than 0.25%, and the turbulence intensity was of the order of 0.5%. The freestream velocity U_o was set at 16.5 m/s, resulting in a Reynolds number based on body length ($Re = U_o L/\nu$) of 1.58×10^6, where ν is the kinematic viscosity of air. The jet velocity was adjusted to obtain the self-propelled condition, that is, such that the axial momentum of the jet was equal to the momentum loss due to the body drag. This condition was achieved with a maximum axial velocity at the jet exit of $U_j = 1.35U_o$.

As shown in Fig. 1, the model was mounted with a part of it extending into the tunnel contraction. This enabled measurements in the axial direction up to $x/D = 19.53$, where x is measured from the base, and up to $r/R = 4.5$ to recover the freestream conditions

Received 11 May 1998; revision received 26 July 1999; accepted for publication 29 August 1999.

*Assistant Professor, Department of Naval Architecture and Marine Engineering. Member AIAA.
†Professor, Department of Mechanical Engineering, and Director, Iowa Institute of Hydraulic Research. Associate Fellow AIAA.

Table 1 Power laws for an axisymmetric momentumless wake

Reference	l	U	$(\overline{uv})_m$	k_m	ε_m	$(\overline{u^2}-\overline{v^2})_m$
Tennekes and Lumley[12]	0.200	−0.800	——	——	——	——
Ferry and Piquet[10]	0.200	−0.800	−1.600	−1.600	−2.600	——
Hassid[9]	0.270	−1.270	——	−0.730	——	——
Finson[8]	0.276	−1.636	−2.364	−1.455	——	−1.636
Sirviente[11]	0.250	−1.500	−2.250	−1.500	−5.500	−1.500

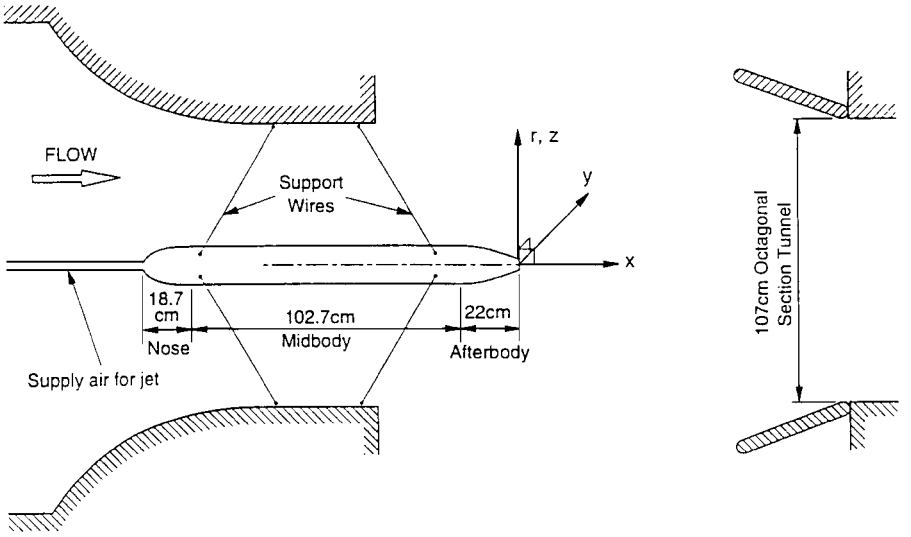

Fig. 1 Wind tunnel and model arrangement.

in the radial direction. Although description of this steady, axially symmetric flow requires measurements along a single radial line at each axial position, measurements were taken across the (vertical) diameter as a check for symmetry. Most of the measurements were made with a triple-sensor hot-wire probe and a five-hole pitot probe. The latter was used to determine the mean-flow direction so that proper yaw and pitch angles for the hot-wire probe could be selected. It also provided redundant data for the mean-velocity components. The probes were traversed in the vertical direction by a simple computer-controlled mechanism.

Detailed description of the experimental equipment, instrumentation, and measurement procedures can be found in Ref. 11, along with an analysis of the uncertainty in the data. There it is shown that the uncertainties of the mean velocity components measured with the hot-wire were less than $0.02U_o$ and those in flow directionality were within ±1.5 deg. Uncertainties of the axial Reynolds stress $\overline{uu}$ and the shear stress $\overline{uv}$ were estimated to be 10%, whereas those of the remaining stresses were 20%. Measurements with the five-hole pitot probe had uncertainties of $0.02U_o$ in velocity magnitude and ±1.5 deg in flow direction.

III. Measurements in Component Flows

Measurements in the boundary layer over the body and in the near wake were previously described by Sirviente and Patel.[1] Therefore, in this section it will be sufficient to indicate that at $x/L=-0.180$, the usual boundary-layer parameters were momentum-thickness Reynolds number, $R_\theta = U_o\theta/\nu = 845$; shape parameter, $H = 1.29$; and friction coefficient, $C_f = 0.0045$. The region of reverse flow extended up to $x/D = 0.551$.

Similar measurements were made in the jet issuing from the tail of the body without any ambient flow. With the jet axial momentum adjusted to equal the bare-body drag, the jet Reynolds number Re_j ($=U_jD/\nu$) was 5.7×10^4, with $U_j = 22.27$ m/s. The streamwise development of the jet may be described in three parts; a region up to about $x/D=4$, where the centerline velocity and the jet radius remain essentially constant; a region farther downstream $x/D>10$ in which the half-radius b increases linearly with x and the centerline velocity U_c decreases as x^{-1} (as predicted by similarity analysis); and an intermediate zone between the two. The jet virtual origin, located by extrapolation of b to the axis is at $x_o/D=-0.56$, and the half-angle of jet spread is 5.88 deg. Further discussion related to the isolated jet can be found in Ref. 11.

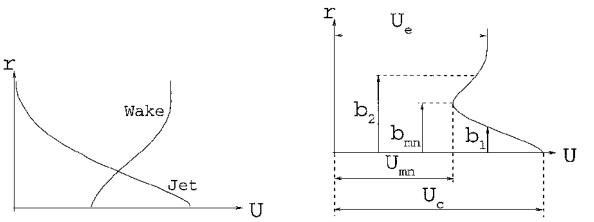

Component flows **Combined flow**

Fig. 2 Typical axial U velocity profile in a momentumless wake.

IV. Momentumless Wake

A. Mean Flow

Figure 2 shows typical velocity profiles in the component flows, namely, the drag wake and the jet, and the velocity profile in the combined flow, the momentumless wake. It is clear that the latter is characterized by three velocity scales, U_c, U_{mn}, and U_e, and three length scales, b_1, b_{mn}, and b_2. The scale b_1 corresponds to the radial location where the velocity is $(U_c-U_{mn})/2$, b_2 to $(U_o-U_{mn})/2$, and b_{mn} to U_{mn}. Because the velocity outside the wake U_e differed from the constant freestream velocity U_o only in a short region close to the body, it is not considered further as a significant variable. Also, because the flow develops downstream, the differences in the mean velocity become small and determination of length scales from the mean-velocity profile becomes progressively inaccurate. Therefore, length scales based on turbulence profiles, defined in Sec. IV.B, are used.

Figure 3 shows velocity profiles at six representative streamwise stations, designated A–F, where the velocity is normalized by U_o and the streamwise distance by R and in some figures by the body

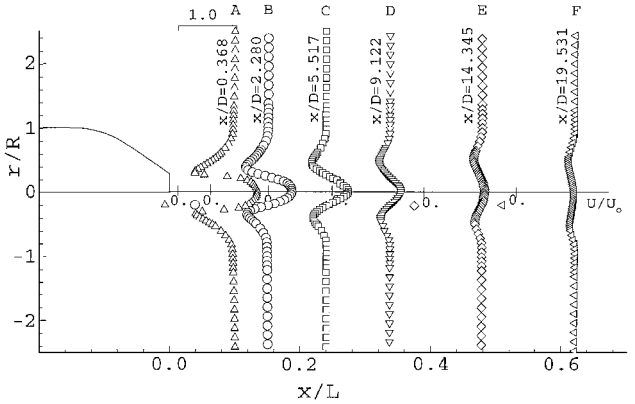

Fig. 3 Mean axial velocity profiles.

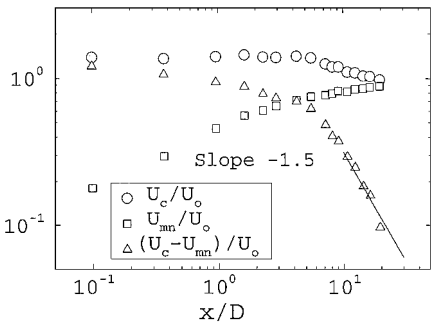

Velocity

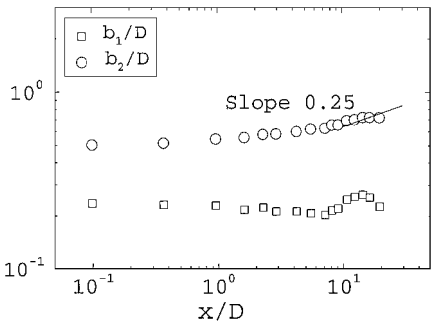

Length

Fig. 4 Wake velocity and length scales.

length L to facilitate comparisons with the results of the drag (bare-body) wake. The velocity profiles clearly show the jetlike flow in the central portion of the near wake, surrounded by boundary-layer flow. The velocity excess in the jet and defect in the boundary layer interact to cause a rapid decay of the mean shear. The centerline velocity (Fig. 4) resembles that of the isolated jet (not shown). It remains constant up to $x/D = 4$, decreases thereafter, and approaches the freestream velocity, being $1.02U_o$ by the last measurement station. The minimum velocity, on the other hand, increases rapidly in the same initial region and more gradually thereafter to approach the freestream velocity, being $0.88U_o$ at the last station. Thus, by the last measurement station, the velocity variations across the entire wake are small. Comparisons with the maximum velocity defect in the drag wake and the centerline velocity of the isolated jet indicate that the mean shear and, therefore, the rate of turbulence production are considerably smaller in the momentumless wake than in the component flows. The half-radius b_1 (Fig. 4) increases very slowly along the wake compared with that of the isolated jet (not shown). This is due to the confinement imposed by the boundary layer surrounding the jet. The length scale b_2, which is a characteristic of the boundary layer, also increases.

Figure 4 also compares the measured evolution of the velocity and length scales with the similarity results of Sirviente[11] (see Table 1). Clearly the individual velocities do not follow any of the predicted power laws. Rather surprisingly, the velocity difference $(U_c - U_{mn})/U_o$, which is more representative of the core of the wake, follows the -1.5 power law predicted by similarity theory. Of the two length scales, only the outer one, b_2, appears to follow the predicted 0.25 power law. However, as already noted, determination of these lengths from experimental data in the far wake is subject to considerable uncertainty.

Three zones were distinguished[1] in the evolution of the drag wake: an initial narrowing, followed by an intermediate region, and finally a zone where the similarity laws applied. In the momentumless wake, however, the interaction between the jet and the wake constrains the jet from spreading radially outward, as shown by the development of b_1, and destroys the original region where the wake width narrows, as shown by b_2, leaving the wake width practically unchanged in the near field, $x/D < 4$. This initial region, where the main characteristics of the jet are unaffected by the boundary layer outside it, is followed by an intermediate zone ($4 < x/D < 12$), where the mixing between the jet and the boundary layer spreads to the wake centerline. Beyond $x/D = 12$ lies the region where limited similarity is observed. The overall flow development was found to be very similar to that of the isolated jet.

Analysis of the evolution of the mass-flux deficit defined as

$$\int_0^\infty \left(1 - \frac{U}{U_o}\right)\frac{r}{R}\,\mathrm{d}\left(\frac{r}{R}\right) = m_x \tag{1}$$

shows[11] that there is a very rapid decrease of the mass deficit in the near wake due to entrainment of the inviscid fluid by the boundary layer. Surprisingly, the mass-flux deficit vanishes beyond $x/D = 9$, indicating no entrainment in the developed region of the momentumless wake. Analogously, the three terms in the axial momentum integral equation, the convective, turbulence, and pressure terms:

$$\int_{-\infty}^\infty \left(1 - \frac{U}{U_o}\right)\frac{U}{U_o}\frac{r}{R}\,\mathrm{d}\left(\frac{r}{R}\right) - \int_{-\infty}^\infty \frac{\overline{uu}}{U_o^2}\frac{r}{R}\,\mathrm{d}\left(\frac{r}{R}\right)$$

$$-\frac{1}{2}\int_{-\infty}^\infty \frac{p}{\rho U_o^2|_2}\frac{r}{R}\,\mathrm{d}\left(\frac{r}{R}\right) = 0 \tag{2}$$

were studied,[11] showing that by approximately $x/D = 9$, all three terms become negligible. In the near and intermediate regions, the contributions from mean-flow convection and pressure are nearly equal and opposite, with convection by turbulence remaining negligible throughout. All along the wake, the net flux of axial momentum deviates from zero by no more than 0.01.

B. Turbulence and Approach to Similarity

Distributions of the turbulence kinetic energy k and the only nonzero shear stress $\overline{uv}$ are presented in Figs. 5 and 6, respectively. The characteristic intensity and length scales of their profiles are also shown in Fig. 7. These include the maximum values k_m, $\overline{uu}_m$, and $\overline{uv}_m$ and the radius $b_{\overline{uu}_{m/2}}$ where $\overline{uu}$ is one-half its maximum value.

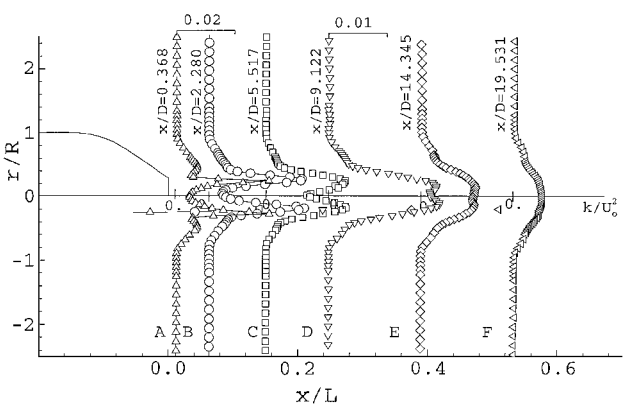

Fig. 5 Turbulence kinetic energy profiles.

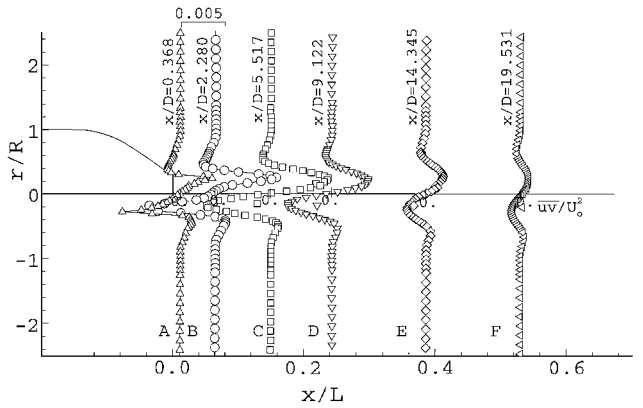

Fig. 6 Shear stress, $\overline{uv}/U_o^2$, profiles.

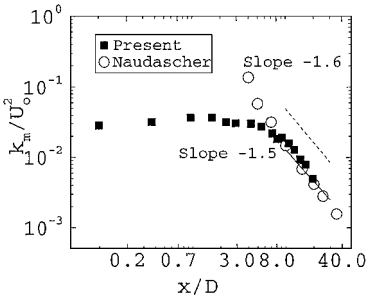

a) Turbulence kinetic energy

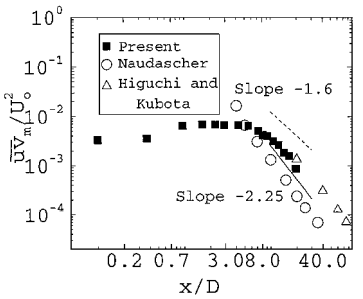

b) Shear stress

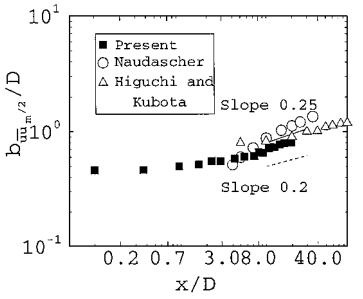

c) Length scale

Fig. 7 Decay of turbulence intensity and length scales in momentumless wakes.

Figure 7 shows that the peak turbulence kinetic energy increases up to $x/D = 2$ and gradually decreases thereafter. The centerline value was found to remain unchanged up to $x/D = 4$. The latter results are similar to those in an isolated jet and suggest that the jet core is preserved for about 4 diameters. On the other hand, the earlier decrease of k_m indicates more rapid mixing in the shear layer surrounding the jet. By approximately $x/D = 12$, k_m occurs at the centerline indicating mixing of the shear layer across the wake. The normal stress (not shown) distributions were found to be similar to those of k, but the maximum of $\overline{uu}$ did not occur at the centerline until the last measurement station. This underscores the difficulty of precisely defining the origin of the momentumless wake as a single shear flow. The shear stress distributions of Fig. 7 clearly show the shear layer in the near wake and sign changes expected from the changes in the mean velocity gradients. The maximum value starts to decay from approximately the station where the turbulence kinetic energy is maximum. Although $b_{k_m/2}$ would appear to be a good choice for a length scale, especially in view of the importance of k in turbulence models and in similarity analysis, previous studies have employed $b_{\overline{uu}_m/2}$ because its determination does not require measurement of all three normal stresses.

Figure 7 shows not only the various velocity and length scales of the turbulence profiles in logarithmic plots, but also their comparisons with some of the power laws of Table 1. First, it is seen that all scales follow these power laws beyond $x/D = 12$ somewhat better than the scales of mean velocity profiles. Second, the data are in better agreement with the power laws deduced by Sirviente[11] than those of Ferry and Piquet.[10] Production of turbulence was neglected in the former analysis, whereas the latter was based on the assumption of equilibrium between production and dissipation. Comparison of the results for the momentumless wake (Fig. 7) with those of the drag wake[1] and the jet (not shown) clearly shows a more rapid decay of turbulence in the momentumless wake due to the decrease in production.

Comparisons with the data of Naudascher[5] and Higuchi and Kubota[7] are also provided in Fig. 7. The differences in the near field are obviously related to the vastly different initial conditions in the experiments; Naudascher[5] used a circular disk as the wake generator whereas Higuchi and Kubota used a thin-wall tube. Similarity theory requires the data to follow the same power laws in the far wake, however. Although comparison of Fig. 7 with Fig. 4 shows that the intensity and length scales of turbulence show somewhat better correlation than those of mean velocity, there persist systematic differences between Naudascher's data and the other two sets. That the present data are in agreement with those of Higuchi and Kubota[7] in almost all respects, and both are in better agreement with the power laws predicted by similarity analysis, suggests that Naudascher's results[5] continue to be influenced by initial conditions (and much longer distance may be required for them to achieve similarity).

The approach to similarity of the mean velocity and turbulence profiles at the most downstream stations is explored in Fig. 8. The radial distance is made dimensionless by $b_{\overline{uu}_m/2}$, following previous studies in momentumless wakes. The velocity profiles are plotted twice, showing the distributions of $(U - U_{mn})/(U_c - U_{mn})$ and $(U - U_{mn})/(U_o - U_{mn})$, whereas $\overline{uu}$ and $\overline{uv}$ are normalized by their maximum values. The velocity profiles reveal the central difficulty of similarity analysis, which assumes a single velocity scale, whereas the results indicate that the inner and outer parts of the momentumless wake scale on different velocity scales, namely, $(U_c - U_{mn})$ and $(U_o - U_{mn})$, respectively. The remarkable collapse of the profiles separately in the two regions, matching at the location of minimum velocity, approximately at $r = 1.2b_{\overline{uu}/2}$, is perhaps the most interesting and intriguing result from Fig. 8. Clearly, this would require a reconsideration of analytical studies based on similarity theory under the usual assumption of a single characteristic velocity scale. Note that both velocity scales, $(U_c - U_{mn})$ and $(U_o - U_{mn})$, tend to zero with axial distance, and their experimental determination is subject to considerable error. The profiles of the normal stress in Fig. 8c appear to indicate a tendency toward similarity, but this is somewhat deceptive. Greater insight is provided by the shear stress profiles of Fig. 8d. There are two peaks in the shear stress, one in the inner region and another of opposite sign in the outer region. Figure 8d uses the maximum value occurring in the inner region. Therefore, the collapse of the profile from the centerline to the point of zero stress (roughly coincident with U_{mn}) simply confirms the similarity of the inner region noted from Fig. 8a. When the profiles were normalized by the peak value in the outer region, they collapsed in the outer region. Thus, these profiles also allude to the need for two velocity scales to describe the momentumless wake.

V. Mixing Between the Jet and Boundary Layer

In the preceding section attention was focused on major features of streamwise flow development. With this accomplished, it is useful to review some (due to space restrictions) of the data at a few selected

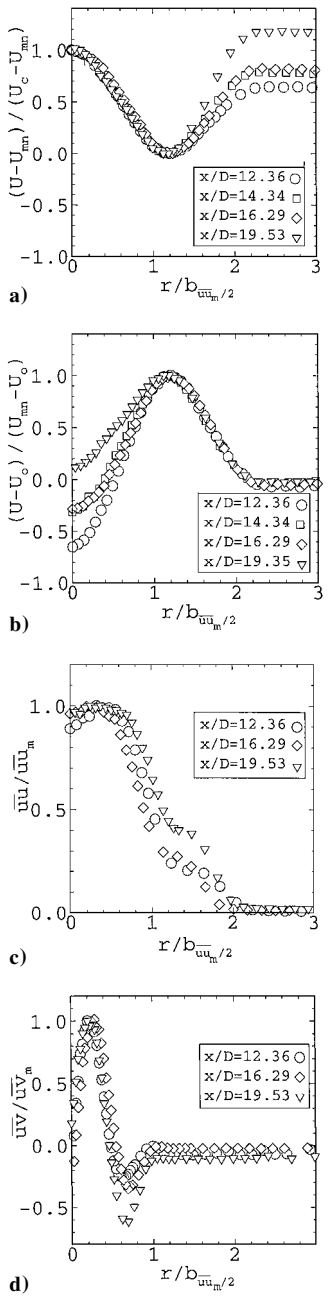

Fig. 8 Similarity of velocity and turbulence profiles.

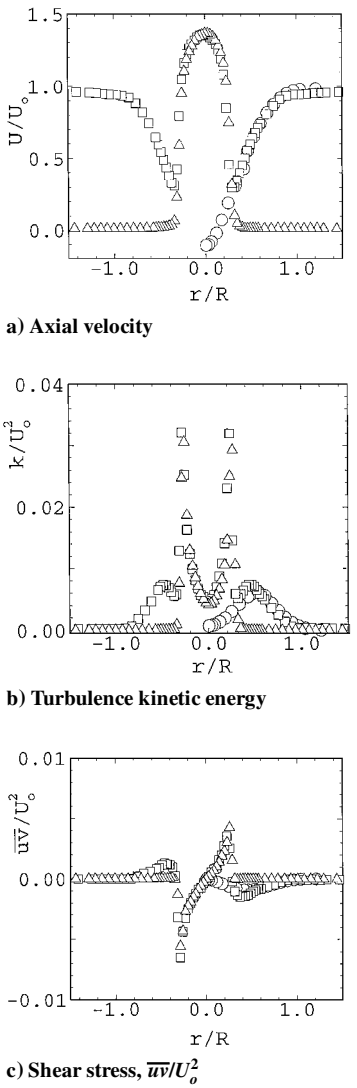

Fig. 9 Measurements at station A: ○, wake; △, jet; and □, momentumless wake.

stations to further investigate the mixing between the jet and the boundary layer. Figures 9–11 show the measurements at stations A, B, D, and F. Each of Figs. 9–11 is in three parts, showing profiles of the mean velocity component U, turbulence kinetic energy k, and shear stress $\overline{uv}$. Also, each of Figs. 9–11 shows the measurements at the same locations in the drag wake, the jet, and their combination, that is, the momentumless wake. All quantities are normalized by the constant scales U_o and R, although it is recognized that the free-stream velocity has no significance in the isolated jet. Data obtained from a vertical traverse of the probes, on both sides of the flow axis, are plotted to show the level of symmetry achieved in the experiments. With the exception of the pressure at all stations, which was measured with the five-hole pitot probe, and the velocity and turbulence data at station A in the drag wake measured with the laser Doppler velocimeter (LDV), all data were obtained with the triple-sensor hot-wire probe.

For these axisymmetric flows, the tangential velocity W and two ($\overline{uw}$ and $\overline{vw}$) of the three shear stresses should be zero. Also, the radial velocity V and the remaining shear stress $\overline{uv}$ should be antisymmetric across the flow. Not all of these conditions were precisely realized in the experiments. However, the observed departures from the expected conditions are, in general, within the limits of experimental uncertainty, especially if probe interference and measuring-volume effects in the shear layers in the near field (stations A and B) are taken into account. Lack of perfect symmetry of the flows also cannot be discounted. Therefore, the observed departures from the requirements of axial symmetry of the three flows should be viewed as a measure of the overall reliability of the complete database. Thus, no further discussion is necessary of the quantities that should be zero.

Station A (Fig. 9), at $x/D = 0.38$ from the body tail and the jet exit, lies in the separated flow region of the bare-body wake and in the core region of the isolated jet. A cursory examination of Fig. 9a would suggest that the momentumless wake at this station is a simple superposition of the two component flows, with measurements in the momentumless wake agreeing with those in the jet in the region $r/R < 0.3$ and with the pure wake in $r/R > 0.3$. This concept, although useful, hides differences that are not immediately apparent from Fig. 9a. For example, the profile of the radial component of velocity and the pressure coefficient (not shown) would suggest that the effect of the jet in the core of the momentumless wake is felt farther than that of the separated flow region in the bare-body wake, implying different entrainment and growth rates of the shear layer emanating from the lip of the jet orifice located at $r/R = 0.35$. The pressure decrease in the bare-body wake in $r/R > 0.8$ was attributed to the velocity at the edge of the wake U_e being less than U_o. The pressure distribution across the momentumless wake suggested that the change in the flow near the base is felt deeper into the inviscid region, as is seen from the velocity profiles in Fig. 9a.

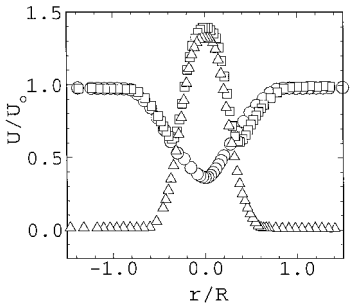

a) Axial velocity

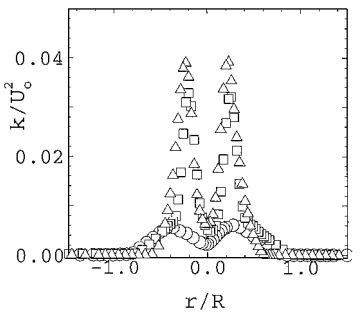

b) Turbulence kinetic energy

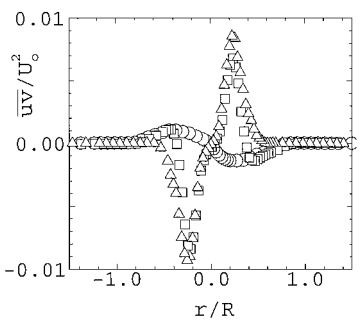

c) Shear stress, $\overline{uv}/U_o^2$

Fig. 10 Measurements at station B: ○, wake; △, jet; and □, momentumless wake.

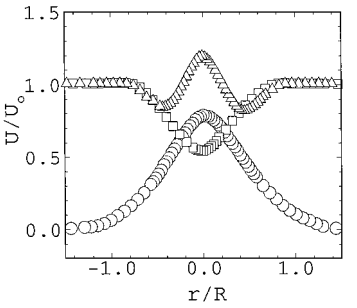

a) Axial velocity

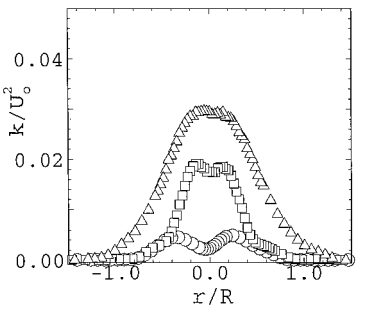

b) Turbulence kinetic energy

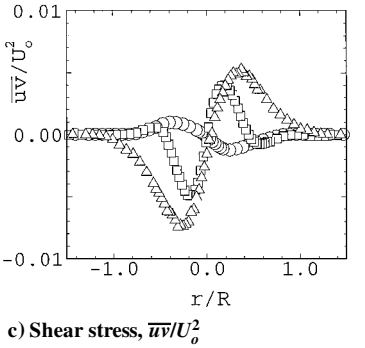

c) Shear stress, $\overline{uv}/U_o^2$

Fig. 11 Measurements at station D: ○, wake; △, jet; and □, momentumless wake.

The shear layers in the three flows are easily identified by the peaks in the turbulence quantities shown in Figs. 9b and 9c. The shear layer of the isolated jet and that of the momentumless wake are, of course, considerably more intense than that of the bare-body wake, as is evident from the peak values of all turbulence quantities. Once again, the concept of superposition is useful in that the turbulence in the wake core resembles the flow in the jet whereas that in the outer part resembles the flow in the bare-body wake. The dividing line is around $r/R = 0.3$.

The measurements at station B, at $x/D = 2.28$, are shown in Fig. 10. This station corresponds to the recovery from separation in the bare-body wake and the end of the core region of the isolated jet. The axial velocity profile shows a behavior similar to that at the previous station insofar as the inner and outer regions of the momentumless wake agree, respectively, with the jet and wake data. However, the centerline velocity is increased in comparison with that of the isolated jet. Also, the concept of superposition is no longer valid as is clear from the turbulence data that show that the jetlike region is considerably narrower as a result of the confinement imposed by the surrounding boundary layer. This narrowing of the jet is apparent from the location of the minimum axial velocity (Fig. 10a) as well as the distributions of the kinetic energy (Fig. 10b) and the shear stress (Fig. 10c). The maximum level of turbulence kinetic energy measured in the momentumless wake is comparable to that found at station A, but much smaller than in the isolated jet. On the other hand, the centerline value is the same as that in the jet, implying that the mixing between the boundary layer and the jet has not reached the centerline. The maximum of the axial normal stress is significantly reduced in comparison to the maximum values of the radial and tangential normal stresses, indicating different anisotropy levels in the shear layers of the two flows. The considerably lower intensity of the shear layer of the bare-body wake is also apparent from the peak values of all turbulence quantities.

Station D, at $x/D = 9.12$, lies in what was termed the transition or intermediate regions of the two component flows, downstream of the core region of the jet and the near field of the bare-body wake. The data presented in Fig. 11 clearly show that the flow structure is vastly different from that at the preceding two stations. The centerline velocity in the momentumless wake is $1.2U_o$ compared to $0.8U_o$ in the jet and $0.56U_o$ in the drag wake. The mean shear across the wake is considerably smaller than in the component flows, indicating a lower level of turbulence production. By this station the static pressure variation makes negligible contribution to the momentum balance. The radial velocity component is small in the three flows suggesting that boundary-layer approximations apply equally well to all of them.

The turbulence profiles (Figs. 11b and 11c) show that the diameter of the momentumless wake is comparable to that of the drag wake and much smaller than the isolated jet. Also, the magnitudes of the various turbulence quantities are intermediate to those in the two component flows but closer to those in the jet. The turbulence kinetic energy continues to show a dip at the centerline whereas such a dip is no longer seen in the jet data. This suggests that the shear layer between the jet and the boundary layer in the momentumless wake is not fully merged at the centerline. In other words, this flow continues to show some of the features of the jet at the center.

Measurements at the last station (station F at $x/D = 19.53$, not shown) indicate greatly reduced mean shear compared to the drag

wake and the jet at the same location. The shear stress was comparable with that in the drag wake but considerably smaller than in the jet. The turbulence kinetic energy showed single maxima at the centerline, and its magnitude is generally similar to those in the drag wake but smaller than in the jet. The mixing of the boundary layer and the jet was practically completed, with the diameter of the momentumless wake being comparable with that of the drag wake and almost half of the isolated jet. Note that the drag wake as well as the jet indicated similarity properties at this measurement station whereas the momentumless wake showed limited similarity with respect to the shapes of the velocity and turbulence profiles.

Significant differences were found in quantities such as eddy viscosity, intermittency, triple-velocity correlations, and turbulence length scales at the last measuring station in the three flows. Limitations of space preclude a discussion of these aspects in the present paper.

VI. Conclusions

This paper reports experiments in the momentumless wake of an axisymmetric body propelled by a concentric circular jet. The principal results and conclusions are summarized as follows.

1) These experiments provide a detailed set of data describing the mixing of a jet and a thick boundary layer and their evolution toward a single flow, the axisymmetric momentumless wake. This is one of a very few experiments that relate to mixing of two turbulent shear layers with different velocity and length scales and, as such, should provide valuable insights in the development and validation of turbulence models. This is facilitated by corresponding data in the two component flows.

2) The mixing between the jet and the boundary layer takes place in three stages: in the near field, $x/D < 4$, wherein the two flows preserve their respective characteristics in the inner and outer regions with a growing shear layer separating them; in an intermediate region, where the shear layer penetrates and mixes up to the centerline; and in the final zone of developed flow, $x/D > 12$, wherein the flow acquires some of the characteristics of a single canonical free shear layer, the momentumless wake.

3) Comparisons with previous experiments in axisymmetric momentumless wakes show some similarities in the far wake in spite of significant differences in their origins.

4) Several characteristic scales of the flow in the developed region exhibit power law behaviors predicted by classical similarity analysis. However, the velocity and turbulence profiles clearly indicate the need for two separate velocity scales to describe the inner and outer regions, and quite possibly two length scales, although the evidence for the latter was not conclusive. These results are important for two reasons. First, they suggest that the two component flows do not completely mix. In other words, the momentumless wake retains a memory of its origin far longer than the more common free shear layers. This tends to support the characterization of this flow, by some previous workers,[3–5] as decaying homogeneous turbulence. Second, the need for two velocity scales casts serious doubt on classical similarity analysis that is based on a single velocity scale. It is possible that this flow requires overlap type arguments used in equilibrium boundary layers in which an inner layer is matched to an outer layer in a common region.

5) The mean shear in the developed-flow region of the momentumless wake is considerably smaller than that in the drag wake and the isolated jet at comparable locations, indicating diminishing rates of turbulence energy production. Predictions of similarity theory based on negligible production are in somewhat better agreement with experiments, but the role of such theory in this flow remains questionable.

References

[1]Sirviente, A. I., and Patel, V. C., "Experiments in the Turbulent Near Wake of an Axisymmetric Body," *AIAA Journal*, Vol. 37, No. 12, 1999, pp. 1670–1673.

[2]Sirviente, A. I., and Patel, V. C., "Wake of a Self-Propelled Body, Part 2: Momentumless Wake with Swirl," *AIAA Journal*, Vol. 38, No. 4, 2000, pp. 620–627.

[3]Ridjanovic, M., "Wake with Zero Change of Momentum Flux," Ph.D. Dissertation, Dept. of Mechanical Engineering, Univ. of Iowa, Iowa City, IA, 1963.

[4]Wang, H., "Flow Behind a Point Source of Turbulence," Ph.D. Dissertation, Dept. of Mechanical Engineering, Univ. of Iowa, Iowa City, IA, 1965.

[5]Naudascher, E., "Flow in the Wake of Self-Propelled Bodies and Related Sources of Turbulence," *Journal of Fluids Mechanics*, Vol. 22, Aug. 1965, pp. 625–656.

[6]Schetz, J. A., and Jakubowski, A. K., "Experimental Studies of the Turbulent Wake Behind Self-Propelled Slender Bodies," *AIAA Journal*, Vol. 13, No. 12, 1975, pp. 1568–1575.

[7]Higuchi, H., and Kubota, T., "Axisymmetric Wakes Behind a Slender Body Including Zero-Momentum Configurations," *Physics of Fluids A–Fluid Dynamics*, Vol. 2, No. 9, 1990, pp. 1615–1623.

[8]Finson, M. L., "Similarity Behaviour of Momentumless Turbulent Wakes," *Journal of Fluid Mechanics*, Vol. 71, No. 14, 1975, pp. 465–479.

[9]Hassid, S., "Similarity and Decay Law of Momentumless Wakes," *Physics of Fluids*, Vol. 23, No. 2, 1980, pp. 404–405.

[10]Ferry, M., and Piquet, J., "Sillage Visqueux Lointain d'un Corps Sous-Marin Autopropulse," SIREHNA, Rapport d'Etude 86/14/R, Nantes, France, 1987.

[11]Sirviente, A. I., "Wake of an Axisymmetric Body Propelled by a Jet with and without Swirl," Ph.D. Dissertation, Dept. of Mechanical Engineering, Univ. of Iowa, Iowa City, IA, 1996.

[12]Tennekes, H., and Lumley, J. L., *A First Course in Turbulence*, MIT Press, Cambridge, MA, 1972.

[13]Hyun, B. S., and Patel, V. C., "Measurements in the Flow Around a Marine Propeller at the Stern of an Axisymmetric Body. Part I. Circumferentially-Averaged Flow," *Experiments in Fluids*, Vol. 11, No. 1, 1991, pp. 33–44.

[14]Hyun, B. S., and Patel, V. C., "Measurements in the Flow Around a Marine Propeller at the Stern of an Axisymmetric Body. Part II. Phase-Averaged Flow," *Experiments in Fluids*, Vol. 11, No. 2, 1991, pp. 105–117.

F. W. Chambers
Associate Editor